Direct Capture of Switching Mechanical Wave on IGBT Bare Dies

Libing Bai, Jiahao Wang, Cong Chen, Quan Zhou, Jie Zhang, Lulu Tian, Gen Qiu, and Yuhua Cheng

***Abstract*—Switching mechanical wave (SMW) effect has attracted extensive attention over the past few years owing to its broad application prospects in condition monitoring for insulated gate bipolar transistor (IGBT) devices. Nevertheless, current research focuses on an indirect approach of acoustic emission detection technology to implement the investigation of such phenomenon, which is not conducive to the mechanism revelation of SMW effect and the accurate extraction of its physical characteristics. Herein, an effective detection method based on laser interferometric vibrometer is developed to directly capture SMW on IGBT bare dies. Combining segmented sliding average filtering and empirical mode decomposition, an efficient extraction algorithm is proposed to realize accurate acquisition of weak SMW signal. Based on this method, the dependency relationship between the SMW signal and turn-OFF switching parameters of IGBT chips is investigated with an inductive pulse testing circuit, indicating that the intensity of SMW presents significantly positive correlation with the turn-OFF power dissipation. Moreover, with the aid of electronical scanning platform, field distribution characteristics of SMW are also investigated. This work provides an effective method to realize direct capture of SMW on IGBT bare dies, paving the way to facilitate fundamental exploration of SMW effect in power electronic devices.**

***Index Terms*—Insulated gate bipolar transistor (IGBT) bare dies, laser interferometric vibrometer, on-chip detection, switching mechanical wave.**

I. Introduction

INSULATED gate bipolar transistors (IGBTs) are widely employed as crucial core components in power converter systems due to their low drive power and reduced saturation voltage [1], [2], [3], [4]. As typical switching devices, the electrical characteristics of IGBTs and their correlated mechanical properties under switching conditions deserve priority attention for reliability evaluation. Among a variety of physical procedures involved in IGBT devices, switching mechanical wave (SMW) effect has drawn increasing interest in recent years, due to its great potential for condition monitoring (CM) applications [5], [6]. Compared with traditional CM technologies for power semiconductor devices, such as methods based on electrical parameters [7], [8], thermal parameters [9], [10], and magnetic parameters [11], the method based on the SMW signal captured by acoustic emission (AE) sensors possesses the features of fast response, noninvasiveness, and real-time detection. Therefore, as a supplement to conventional CM methods, SMW-based detection is anticipated to be a promising approach for the monitoring and detecting of mechanical damage, deterioration, and failure for power semiconductor devices. Unlike conventional mechanical stress waves induced by the degradation of packaging materials in power semiconductor devices [12], [13], [14], such as cracking of bond wires, peeling of the solder layer, the SMW is a kind of transient elastic wave occurring at the moments of turn-ON and turn-OFF stages of IGBT devices due to the thermoelastic effect. In other words, as long as the IGBT devices operate under cyclical switching conditions, periodic SMW is bound to be generated simultaneously. Notably, this unique feature makes SMW a promising detection indicator for CM of power electronic devices.

To date, there has been considerable research on the thermoelastic effect. White [15] explored the phenomenon of transient surface heating generating elastic waves through theoretical analysis and experimental verification, discovering that the amplitude of elastic waves is proportional to the absorbed power density, and that the stress wave amplitude is much larger than the radiation pressure under constraint conditions. Morland [16] investigated the thermoelastic stress waves generated by pulsed electromagnetic radiation on the surface of an elastic half-space through theoretical analysis and mathematical modeling, and concluded that compressive stresses are instantaneously generated on the surface for very short pulse durations. Gascoigne and Mcivor [17] analyzed the stress waves generated in a layered medium under transient energy deposition by linear thermoelastic theory and Laplace transforms, and concluded that the maximum stress value depends on the layer thickness ratio, the wave velocity ratio, and the energy deposition function, and that the maximum stress can be significantly affected by optimizing the layer parameters. The above studies focus on revealing the phenomenon of transient heating on elastomer surfaces from the perspective of physics, which has a wide scope of application. However, research on SMW phenomenon induced by thermoelastic effect in IGBT devices is still rare.

Received 29 April 2024; revised 2 August 2024 and 29 September 2024; accepted 9 November 2024. Date of publication 18 November 2024; date of current version 26 December 2024. This work was supported in part by the Fundamental Research Funds for the Central Universities under Grant ZYGX2021J020 and in part by the National Natural Science Foundation of China under Grant 62003074 and Grant U2030205. Recommended for publication by Associate Editor C. DiMarino. *(Corresponding author: Cong Chen.)*

The authors are with the School of Automation Engineering, University of Electronic Science and Technology of China, Chengdu 611731, China (e-mail: libing.bai@uestc.edu.cn; jiahao_wang@std.uestc.edu.cn; cong_chen@uestc.edu.cn; quanzhou@uestc.edu.cn; zhj06_19@uestc.edu.cn; lulutian@uestc.edu.cn; qgen615@uestc.edu.cn; yhcheng@uestc.edu.cn).

Color versions of one or more figures in this article are available at https://doi.org/10.1109/TPEL.2024.3500788.

Digital Object Identifier 10.1109/TPEL.2024.3500788

To be specific, Karkkainen et al. [18] discovered the SMW phenomenon in IGBTs for the first time by means of AE-based detection and showed such an effect could be utilized to realize CM for power semiconductor devices in a follow-up study [19]. Davari et al. [20] proposed a noninvasive method utilizing SMW for detection of power semiconductor aging, and revealed a strong correlation between SMW and ON-state voltage drop from the perspective of spectrum analysis. Bejger et al. [21] adopted the AE detection method to determine and monitor the early stages of damage of switching transistors. Besides, they also carried out how changes in temperature affect the SMW and found that the intensity of SMW is negatively correlated with temperature [22]. Li et al. [23] utilized digital filtering techniques to investigate the SMW effect in IGBT devices and discovered that the low-frequency component of the signal is affected by turn-OFF current. Subsequently, they proposed a novel SMW extraction method based on the differential AE sensor [24], which can decouple the pulse interference mixed in the SMW signal, and investigated the effect of temperature on SMW characteristics [25]. Moreover, they also implemented a theoretical study on the generation mechanism of SMW in IGBT devices [26], indicating that the thermoelastic effect exerts a dominant role in the SMW generation process.

Although these excellent previous investigations promote insight of the SMW effect in power electronic devices, some research gaps need to be further addressed. On the one hand, current research in the SMW effect generally employs AE sensors mounted on the external surface of the packaged power electronic devices to acquire SMW signals. Considering the influence (attenuation and reflection) of functional material layers in the packaging structure on the acoustic transmission of SMW signal arising from IGBT bare dies (generation source), such indirect AE-based detection method is not conducive to the mechanism revelation of SMW effect and the accurate extraction of its physical characteristics. On the other hand, limited by the volume and configuration of AE sensors, the spatial resolution of such an approach is relatively poor, which can hardly achieve the characterization of SMW field distribution characteristics on IGBT bare dies, thus hindering the further exploration of SMW effect. Therefore, there is a great demand to develop an effective detection method for directly capturing SMW on IGBT bare dies without encapsulation, thus facilitating mechanism revelation and fundamental exploration of SMW effect in power electronic devices.

To overcome the above bottlenecks, an effective detection method based on laser interferometric vibrometer is developed to directly capture SMW on IGBT bare dies. Based on this method, segmented sliding average filtering and empirical mode decomposition are performed to accurately extract weak SMW signal, so as to further reveal the dependence relationship between the SMW and switching parameters including switching-OFF moment current, power pulse peak value, and the injected energy of IGBT bare dies. Compared with the current mainstream AE detection approach, this method utilizes laser interference detection to achieve directly non-contact capture of SMW signal on IGBT bare dies, making it possible to study the SMW effect from its initial generation source. Meanwhile, due to the focusable feature of the detection laser beam, high spatial resolution up to tens of microns could be readily achieved, thus realizing the characterization of the field distribution of SMW. The developed ON-chip detection method is bound to facilitate further understanding and fundamental exploration of the SMW effect in power electronic devices. To be specific, by performing real-time frequency analysis of the SMW signal captured by the developed method, the spectral characteristics including frequency range and main components of the SMW signal can be accurately obtained, thus providing reliable bases for the selection of vibration sensors for SMW-based CM of IGBT devices.

The rest of this article is organized as follows. In Section II, the generation mechanism of the SMW effect is analyzed. In Section III, the measurement principle and experimental setup with pulse testing circuit with inductive loading are illustrated in detail. In Section IV, an extraction algorithm is proposed to realize accurate acquisition of weak SMW signal and further to implement comprehensive investigation of SMW. Notably, the impacts of switching conditions including switching-OFF moment current, power pulse peak value, and the injected energy during the switching process are analyzed and discussed in depth. Additionally, the field distribution characteristics of the SMW are also investigated and presented. In Section V, limitations and future work are discussed. Finally, Section VI concludes this article.

II. Mechanism Description

As mentioned above, the SMW is a kind of transient elastic wave, which occurs at the turn-ON and turn-OFF moments of IGBT devices. Due to the power electronic feature of IGBT devices, it is bound to involve the conversion of electrical energy to mechanical energy during such a physical process. Current research finding [26] indicates that thermoelastic effect plays a key role in this electro-mechanical coupling process. It is worth noting that the above viewpoint is applicable to those application scenarios where impulsive energy injection can be triggered in both turn-ON and turn-OFF moments so that SMW can be induced due to thermoelastic effect. While for those application scenarios where impulsive energy injection can only be triggered during turn-OFF switching process, SMW induced by thermoelastic effect are only expected to be observed after turn-OFF moment.

To be specific, during the switching process, the inherent switching loss of IGBT chips is first converted into thermal energy due to the Joule effect. Typically, the energy of the switching loss is on the order of tens of millijoules. However, due to the extremely short duration of the switching process (for instance, the typical turn-OFF duration time is about 1 μs), the converted heat energy will inevitably generate a large transient thermal power pulse excitation (up to tens of kW) on IGBT bare dies. This huge transient thermal pulse excitation necessarily results in a sharp temperature rise, which in turn causes the cell bodies in IGBT bare dies to start forced vibrating due to the thermoelastic effect, which propagates and manifests itself in the form of mechanical stress waves in IGBT devices. The whole physical procedure for SMW effect in IGBT devices is

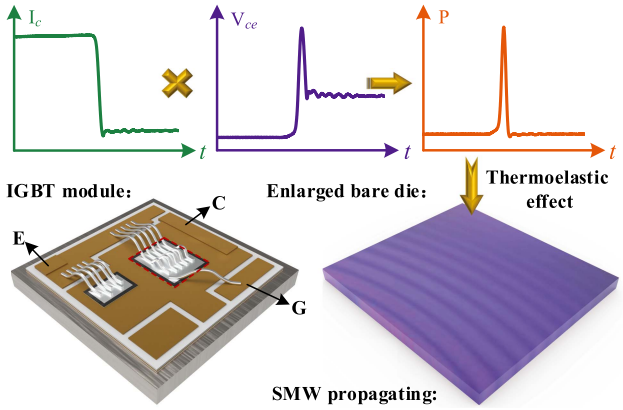

Fig. 1. Schematic illustration of the SMW induced by thermoelastic effect in IGBT devices.

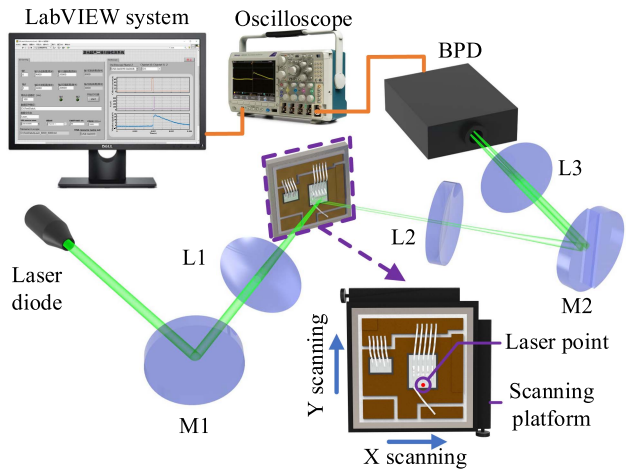

Fig. 2. Diagram of the adaptive laser interferometric vibrometer based detection system for IGBT bare dies.

illustrated in Fig. 1. The above analysis indicates IGBT bare dies are the initial generation source of SMW in packaged IGBT devices. Therefore, realizing direct capture and characterization of SMW on IGBT bare dies is of great significance for mechanism revelation of the SMW effect and the accurate extraction of its physical characteristics in IGBT power devices.

III. Method and Experiment

A. Measurement Principle

The schematic illustration of the developed adaptive laser interferometric vibrometer-based detection system is depicted in Fig. 2. First, a wavelength of 532 nm detection laser beam is generated by a laser diode and then focused by a lens (L1) into a light spot on the surface of IGBT bare dies. Then, the reflected laser beam containing vibration information of the bare die is refocused through another lens (L2) onto an adjustable beam splitter (M2), which splits the reflected laser beam into two detection beams. Subsequently, the two split detection beams are refocused to induce interference through a lens (L3). Afterwards, the interfered light intensity carrying

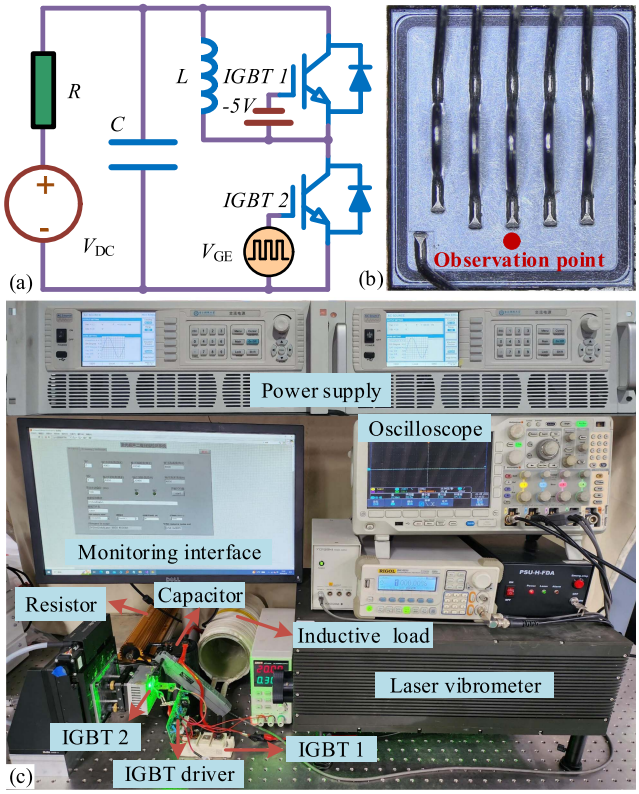

Fig. 3. (a) Pulse testing circuit with inductive loading. (b) Schematic illustration of observation point on bare die of IGBT 2. (c) Experimental platform for the observation of SMW signal under pulse testing circuit with inductive loading.

vibration information is received and transduced by the balanced photoelectric device. Finally, the acquired SMW signal is transmitted to the LabVIEW-based upper monitoring interface. Notably, an electronically controlled positioning and scanning platform is adopted to realize characterization of the SMW field distribution characteristic on IGBT bare dies. The bandwidth of the developed detection system is up to 100 MHz. Considering the high frequency components of the SMW signal could not normally exceed 10 MHz [13], [23], [27], thus, this detection bandwidth is high enough to resolve the transient SMW signal.

B. Experimental Setup

The pulse testing circuit with inductive loading is illustrated in Fig. 3(a). First, a set of single-phase programmable power supply is connected in parallel with a large energy storage capacitor to provide the strong current. Second, a power resistor R is adopted in series with the power supply in the testing circuit to avoid overcurrent, which may induce unnecessary damage to the power supply and components in the circuit. Third, a noncontact caliper current sensor with model 701933 from YOKOGAWA is utilized to realize accurate load current measurement. Fourth, a commercially purchased IGBT power module SKM75GB128D with half-bridge structure from SEMIKRON is utilized for the following experimental investigation. Fifth, the IGBT 2 under test is mounted on an electrical positioning and scanning platform for precise positioning of vibration observation. The

observation point is shown in Fig. 3(b). Finally, the gate voltage is generated by a commercially purchased IGBT universal driver board, which also enables collector and emitter voltage detection and overshoot self-protection function, thus protecting the IGBT device from breakdown due to the voltage overshoot. The whole system containing the laser vibrometer-based detection system and the testing circuit is configured on an optical table to avoid the external vibration interference. The practical experimental setup is shown in Fig. 3(c).

IV. Results and Discussion

Based on the aforementioned method, this section aims to develop an effective extraction algorithm to realize accurate acquisition of weak SMW signal and further implement comprehensive investigation of SMW. The whole section contains four parts, including observation of the SMW signal, extraction algorithm for SMW, impacts of switching parameters on SMW intensity, and field distribution characteristic of SMW, which are illustrated in detail as follows.

A. Observation of SMW Signal

In order to verify the effectiveness of the developed detection system, the detection laser beam is focused into a testing point on the IGBT bare die to observe whether SMW exists in the obtained vibration signal. The corresponding electrical switching parameters and the captured vibration signal are depicted in Fig. 4. It can be seen that, as analyzed in the previous mechanism description section, a transient thermal power pulse up to 16.4 kW [as shown in Fig. 4(c)] is generated in the IGBT bare die due to the sharp drop in collector current I_c [as shown in Fig. 4(a)] and the overshoot of voltage between collector and emitter V_{ce} [as shown in Fig. 4(b)]. It is worth noting that in order to accurately capture and demonstrate the waveform details at the moment of switching OFF, the observation window of the oscilloscope is set to be short enough to ensure accurate measurement of the overshoot in the V_{ce} curve and pulse value in the power loss curve, as shown in the insets of Fig. 4.

Moreover, it can be observed that the captured vibration signal on the IGBT bare die presents an overall trend of first rising and then damped oscillating attenuation, as shown in Fig. 4(d). Specifically, this vibration signal contains three components which are slowly varying contour signal, ring decaying transient signal, and sharp electromagnetic interference signal, respectively. It is worth noting that the ring decaying transient signal starts precisely at the moment of switching OFF with a duration time about 0.31 ms. By comparison with previous research results about SMW in IGBTs utilizing AE technology [18], [24], [25], [26], the above signal features including damped oscillating attenuation, duration time, and moment of appearance indicate that the ring decaying transient signal should be SMW signal induced by thermoelastic effect.

It is worth noting that this indirect comparison has its own feasibility and validity. To be specific, from the physical perspective, both the ring decaying transient signal captured by the proposed method and the SMW signal measured by the AE detection method in previously published literatures are

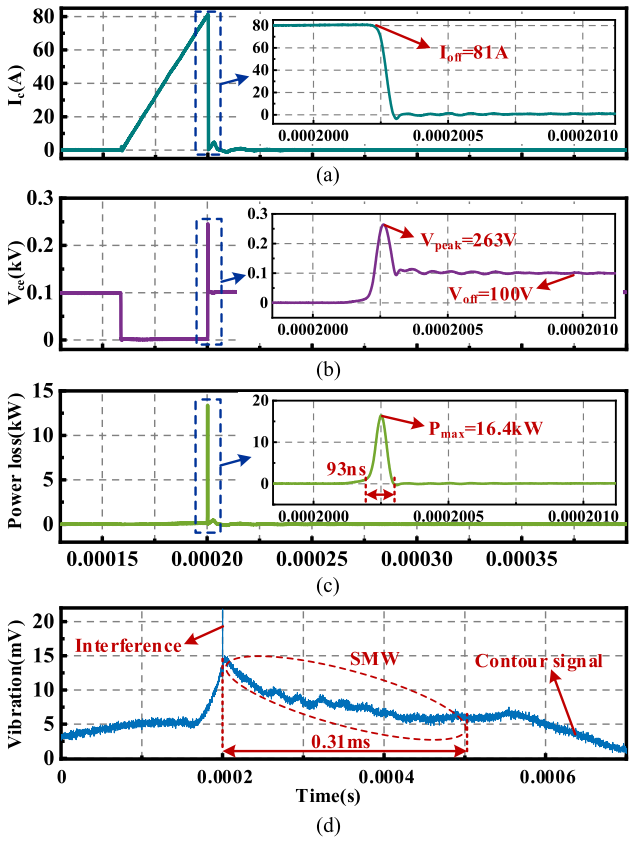

Fig. 4. (a) Collector loading current. (b) Voltage between collector and emitter. (c) Power dissipation. (d) Captured vibration signal of a testing point on IGBT bare die.

essentially the same kind of mechanical vibration signal. In light of this, the above two vibration signals are comparable. However, it should also be noted that the captured ring decaying transient signal corresponds to the vibration signal on the IGBT bare die, which is the source of vibration for the entire IGBT module. Nevertheless, the measured vibration signal by the AE detection method corresponds to the external surface of the IGBT module after attenuation and reflection induced by the above vibration source in the propagation process. Obviously, the above two vibration signals cannot be compared directly in terms of the intensity of the signals, but should be compared from the three features including damped oscillating attenuation, duration time, and moment of appearance. Eventually, from the actual comparison results, the ring decaying transient signal captured by the proposed method and the vibration signal measured by the AE detection method in previously published literature [18], [24], [25], [26] are in good accordance in the above mentioned three features including damped oscillating attenuation, duration time, and moment of appearance, which indicates the feasibility and validity of such indirect comparison to a certain extent.

In order to further verify the consistency of the above obtained characteristics on SMW signal, another five observation points on the IGBT bare die are selected and corresponding vibration signals are also measured, as shown in Fig. 5. The results show that the vibration signals at the five observation points exhibit a

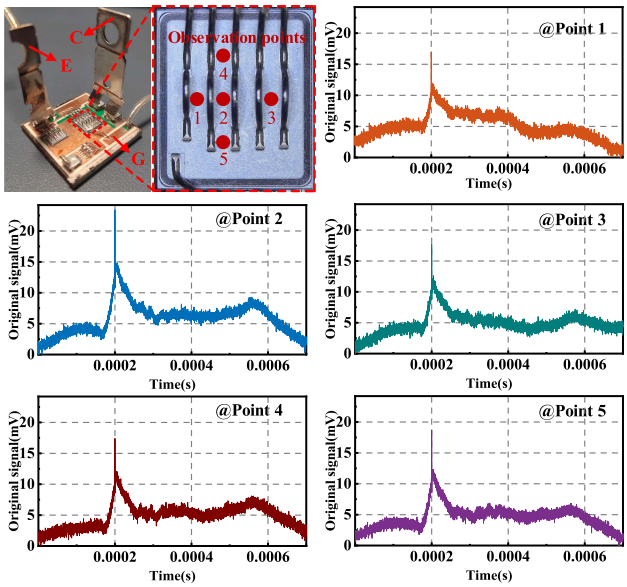

Fig. 5. Selected another five observation points on IGBT bare die and corresponding captured vibration signals.

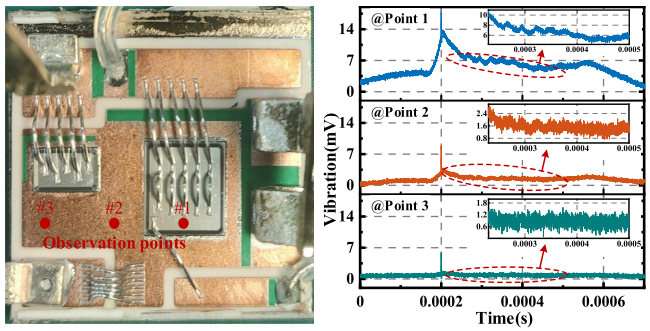

(a) (b)

Fig. 6. (a) Observation points located on IGBT die (#1) and other observation points of the module (#2 and #3). (b) Captured vibration signals at observation points #1, #2, and #3, respectively.

high degree of consistency with the previous conclusions. In order to verify that the origin of the SMW originates from the IGBT bare die, the SMW signals at some other observation points of the module other than on the bare die are also captured, as shown in Fig. 6. It can be seen that among the three observation points, the farther away from the IGBT bare die, the weaker the SMW signal becomes, which suggests that the SMW exhibits a gradual attenuation trend from near to far, thus supporting the viewpoint that the origin of the SMW is from the IGBT die. Finally, the above analysis shows that thermoelastic effect-induced SMW does exist in the IGBT bare die and the developed on-chip detection method based on laser interferometric vibrometer is intuitive and effective.

B. Extraction Algorithm for SMW Signal

The results in the previous section show that the vibration signal captured by the developed detection system is not pure SMW signal, but a mixture of the SMW signal and two other components, which is not conducive to the subsequent investigation of the SMW effect. Therefore, there is a need to develop an efficient signal separation algorithm to achieve accurate extraction of the SMW signal. Herein, an effective extraction algorithm combining segmented sliding average filtering (SSAF) and empirical mode decomposition (EMD) is proposed to realize accurate acquisition of weak SMW signal. The strategy of the proposed algorithm is to first separate the relatively low frequency contour signal component from the original mixed vibration signal by SSAF, and then realize the separation of SMW signal and interference noise from the remaining signal with the help of EMD, thus achieving the extraction of pure SMW signal from the original mixing signal.

To be specific, the original mixing signal can be expressed as

$$s_1(t) = s_2(t) + s_3(t) \tag{1}$$

where $s_2(t)$ is the slowly varying contour signal, $s_3(t)$ is the mixture signal containing SMW signal and electromagnetic interference noise signal. Summing the signal values at adjacent moments within sliding time window w and averaging them give

$$p(t) = \frac{\sum_{i=1}^{\frac{w}{2}} [s_1(t-i) + s_1(t+i)] + s_1(t)}{w+1} \tag{2}$$

where $p(t)$ is the smoothing result. Substituting (1) into (2) yields (3), which is shown at the bottom of the page.

As the mean value of $s_3(t)$ is close to 0, thus, the following relation exists:

$$\frac{\sum_{i=1}^{\frac{w}{2}} [s_3(t-i) + s_3(t+i)] + s_3(t)}{w+1} \approx 0. \tag{4}$$

Therefore, (3) shown at the bottom of this page, can be simplified as

$$p(t) \approx \frac{\sum_{i=1}^{\frac{w}{2}} [s_2(t-i) + s_2(t+i)] + s_2(t)}{w+1}. \tag{5}$$

Based on the abovementioned analysis, it can be seen that the size of sliding time window w has a major influence on the smoothing result. Specifically, a short time window makes the smoothing result closer to the original signal waveform, while a long time window enables the smoothing effect better. Considering that the SMW signal occurs after the switching-OFF moment t_1, thus, the original mixing signal $s_1(t)$ is divided into two separate segments using the switching-OFF moment as the boundary. Specifically, the left segment contains only the relatively high frequency electromagnetic interference signal, so a short sliding time window w_1 can be adopted to obtain the left part of contour signal component. The right segment contains relatively low frequency SMW signal in addition to relatively high frequency electromagnetic interference signal, so a long

$$p(t) = \frac{\sum_{i=1}^{\frac{w}{2}} [s_2(t-i) + s_2(t+i)] + s_2(t) + \sum_{i=1}^{\frac{w}{2}} [s_3(t-i) + s_3(t+i)] + s_3(t)}{w+1}. \tag{3}$$

sliding time window w_2 is required to filter out the SMW signal and obtain the right part of contour signal component. In general, with the aid of the above segmented sliding average filtering, the slowly varying contour signal $s_2(t)$ is firstly obtained.

The next procedure is to utilize EMD to separate SMW signal and electromagnetic interference signal. First, the previously obtained contour signal is removed from the original mixing signal to obtain a mixture of the SMW signal and electromagnetic interference signal, i.e.,

$$s_3(t) = s_1(t) - s_2(t). \tag{6}$$

Then, maximum envelope $e_1(t)$ and minimum envelope $e_2(t)$ in the above signal can be fitted by cubic spline function, and their average envelope is calculated as follows:

$$e_3(t) = \frac{e_1(t) + e_2(t)}{2}. \tag{7}$$

Subtracting $e_3(t)$ from signal $s_3(t)$ gives an intermediate signal

$$s_4(t) = s_3(t) - e_3(t) \tag{8}$$

where $s_4(t)$ is required to repeat iterations of (7) and (8) until the condition that $s_4(t)$ is a single component is satisfied. Thus, after k times iteration, the first-order modal component (MC) of $s_3(t)$ is obtained as

$$c_1(t) = s_4^k(t). \tag{9}$$

Thus, the first-order residual component (RC) $r_1(t)$ is obtained by removing the first-order MC from $s_3(t)$ as follows:

$$r_1(t) = s_3(t) - c_1(t). \tag{10}$$

Subsequently, repeating the calculation process from (7)–(10), the other residual MCs $c_2(t)$, $c_3(t)$, …, $c_{n\text{-}1}(t)$ are obtained until the RC $r_n(t)$ is a monotonic function or a constant. Finally, after n times iteration, the original signal $s_3(t)$ can be expressed as

$$s_3(t) = \sum_{1}^{m} c_i(t) + \left[\sum_{m+1}^{n-1} c_i(t) + r_n(t)\right] \tag{11}$$

where $c_i(t)$ is the i order MC and $r_n(t)$ is the final residual component. It is worth noting that the first part of (11) is the relatively high frequency electromagnetic interference component and the second part is the relatively low frequency SMW signal component.

The specific processing flow of the proposed extraction algorithm is illustrated in Fig. 7. To be specific, the slowly varying contour signal is first separated from the original raw data by SSAF, then, the separated slowly varying contour signal is removed from the original raw data to obtain the remaining mixed signal, which only contains the SMW signal and interference noise, and finally EMD is utilized to separate out the interference noise from the above obtained remaining mixed signal, thereby extracting the SMW signal.

The detailed process of EMD is as follows. As shown in Fig. 8, several MCs and a RC are obtained by performing EMD decomposition on the above remaining mixed signal.

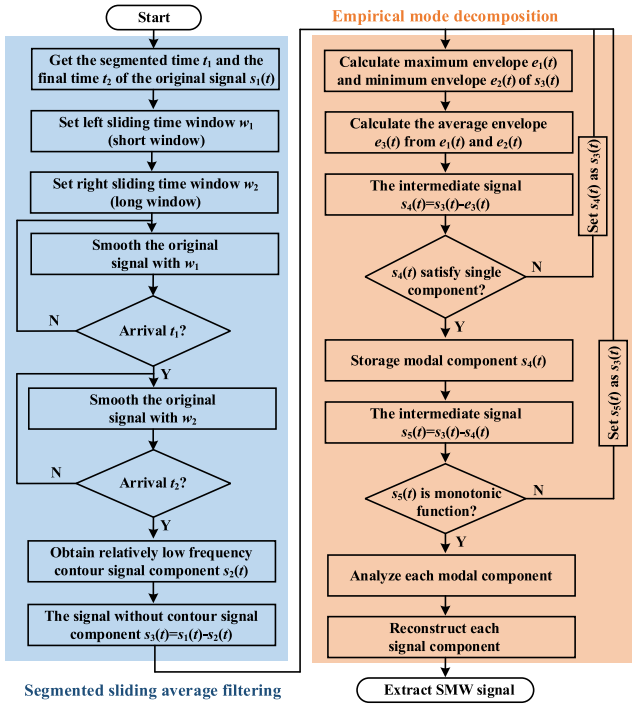

Fig. 7. Extraction algorithm combing segmented sliding average filtering and empirical mode decomposition for SMW signal separation.

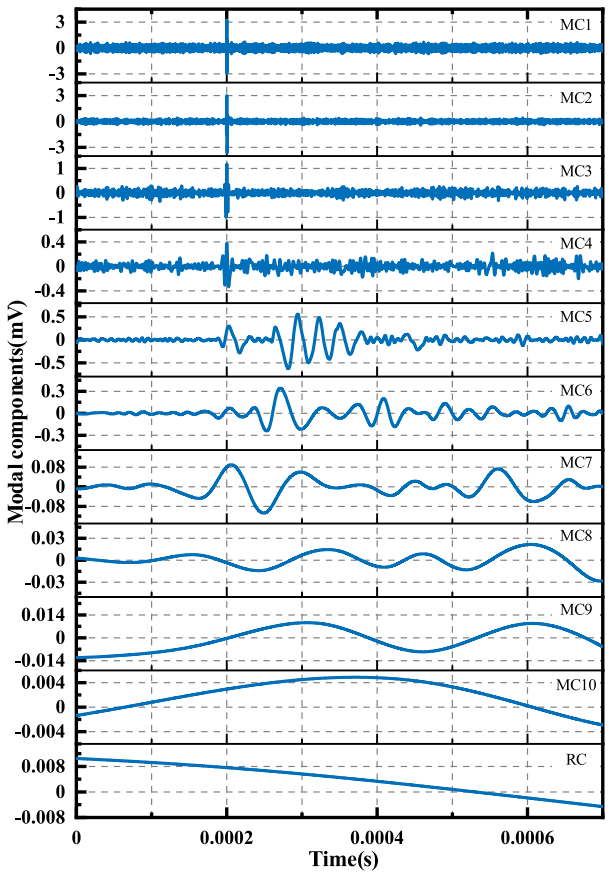

Fig. 8. Each order MCs and RC after EMD.

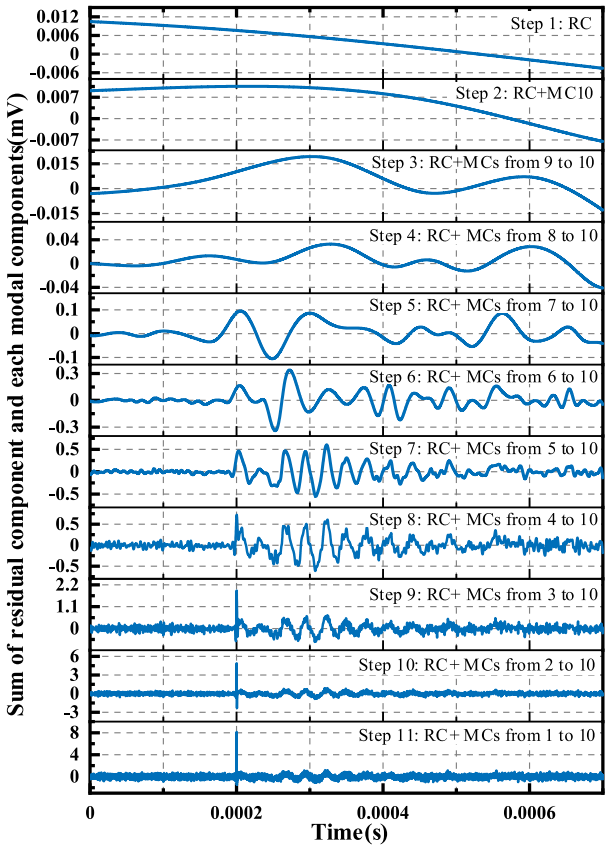

Fig. 9. Process of adding each order MC in turn into the residual component.

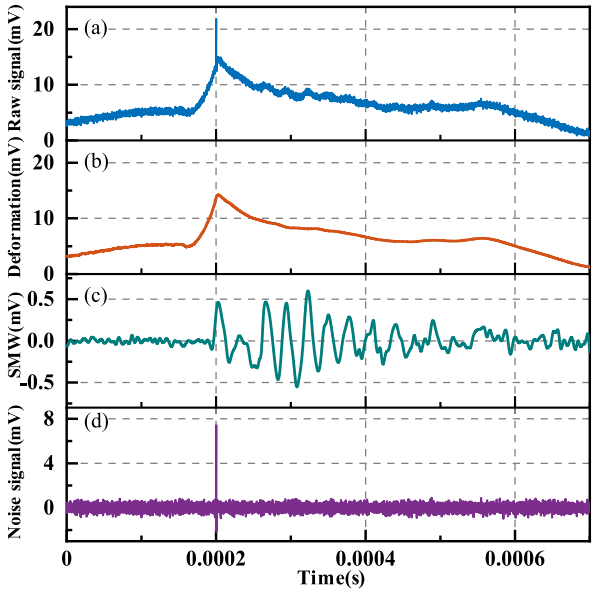

Fig. 10. Demonstration of signal component separation. (a) Original vibration signal. (b) Deformation fluctuation signal. (c) Extracted SMW signal. (d) Electromagnetic interference signal.

However, the SMW signal and the interference signal cannot be directly distinguished from these decomposed MCs and residual component. The solution is to add each obtained MC in turn into the residual component, thus gradually reconstructing the above remaining mixed signal from the low frequency to the high frequency. Then, from the reconstruction process, the contribution of each MC to the remaining mixed signal could be analyzed, thus realizing the identification of the SMW signal and the interference signal.

Fig. 9 shows the reconstructed waveforms after adding each MC step-by-step. It is worth noting that from the reconstruction result between step 7 to 8, it can be seen that after adding MC 4 into RC and MCs from 10 to 5, the reconstructed signal waveform shape remains the same, with only the overlay of little background burr noise. Furthermore, after adding the MC 3, MC 2, and MC 1 to the above reconstructed signal waveform (from step 8 to 11), the interference noise gradually appears. The above analysis shows that the RC and the MCs from 10 to 5 are rightly SMW signal, while the MCs from 4 to 1 are the electromagnetic interference signal with background burr noise. In other words, the parameter m involved in the EMD process is determined to be 4 to achieve the separation of the interference signal and the SMW signal.

The separated signal components are depicted in Fig. 10. First, the slowly varying contour component is separated out, as shown in Fig. 10(b), which is the deformation fluctuation signal caused by thermal expansion effect. To be specific, during cyclical switching process, there exists considerable ON-state and switching loss due to the large loading current, resulting in the temperature swing of the IGBT device via Joule effect. Because of the difference in the coefficient of thermal expansion of each functional layer, the mismatch inevitably leads to the deformation fluctuation due to thermal expansion effect.

Second, ring decaying transient component is extracted afterwards, as shown in Fig. 10(c), which is rightly the SMW signal induced by thermoelastic effect. The corresponding generation mechanism has been explained in the previous section and will not be repeated here. Finally, the sharp electromagnetic interference signal is separated out, as shown in Fig. 10(d), which is induced by space electromagnetic coupling due to large dI_c/dt. It can be seen that the SMW signal extracted by the separation algorithm maintains the characteristics exhibited in the original vibration signal in terms of waveform shape, signal amplitude, and duration time, verifying the accuracy of the proposed extraction algorithm.

To verify the consistency of the detection and extraction results and to eliminate the possibility of coincidence, three samples with same model number are tested and the SMW signals are also extracted adopting the proposed algorithm, as shown in Fig. 11. It can be seen that the extracted SMW signals of the three samples exhibit a high degree of consistency in waveform characteristics, including damped oscillating attenuation, duration time, and moment of appearance. Meanwhile, the discrepancy of captured SMW signals between different samples mainly lies in signal strength, which may be induced by individual difference of samples. It is worth noting that such slight discrepancy is almost inevitable in practical measurement, and does not affect

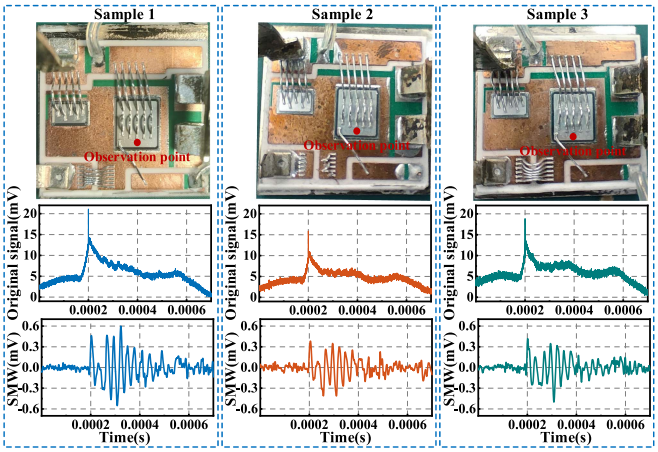

Fig. 11. Captured original vibration signals and extracted SMW signals in three samples with same model number.

the effectiveness and validation of the developed method. Therefore, in light of this, only one sample (Sample 1) is selected for typical demonstration in the subsequent investigation of SMW.

C. Impacts of Switching Parameters on SMW Intensity

As a kind of transient mechanical wave during switching process, switching parameters have significant impacts on the SMW effect. In general, the specific switching parameters contain switching-OFF moment current I_{OFF}, power pulse peak value P_{max}, and the injected energy E_i during pulse excitation.

Gate signals with different pulse width are set to generate different switching-OFF moment current amplitudes corresponding to 39 A, 52 A, 62 A, 72 A, and 81 A to analyze the impacts of switching parameters on SMW intensity, as shown in Fig. 12(a). Corresponding voltage and power dissipation curves of IGBT 2 bare die are exhibited in Fig. 12(b) and (c). It is worth noting that the area enveloped by the pulse and the time axis in the power loss curve is the injected energy into the IGBT bare die. In other words, the injected energy can be calculated by

$$E_i = \int_{t_1}^{t_2} P(t)dt \tag{12}$$

where $P(t)$ represents the power loss of IGBT bare during switching-OFF process, t_1 is the pulse starting moment, and t_2 is the moment when the pulse decays to zero. It can be seen that the peak value of power pulse and the injected energy increase with the growth of ON-state loading current, i.e., they are positively correlated with the ON-state current. Subsequently, the corresponding SMW signals under different switching conditions are also extracted and illustrated in Fig. 12(d), indicating a clearly positive correlation between the intensity of SMW signal and the switching-OFF moment current and power pulse peak value. Furthermore, in order to intuitively demonstrate the influence of switching parameters on SMW intensity, the dependency relationships of SMW signal amplitude, peak-to-peak value, and energy with switching-OFF moment current I_{OFF}, power pulse peak value P_{max}, and injected energy E_i are extracted, as shown

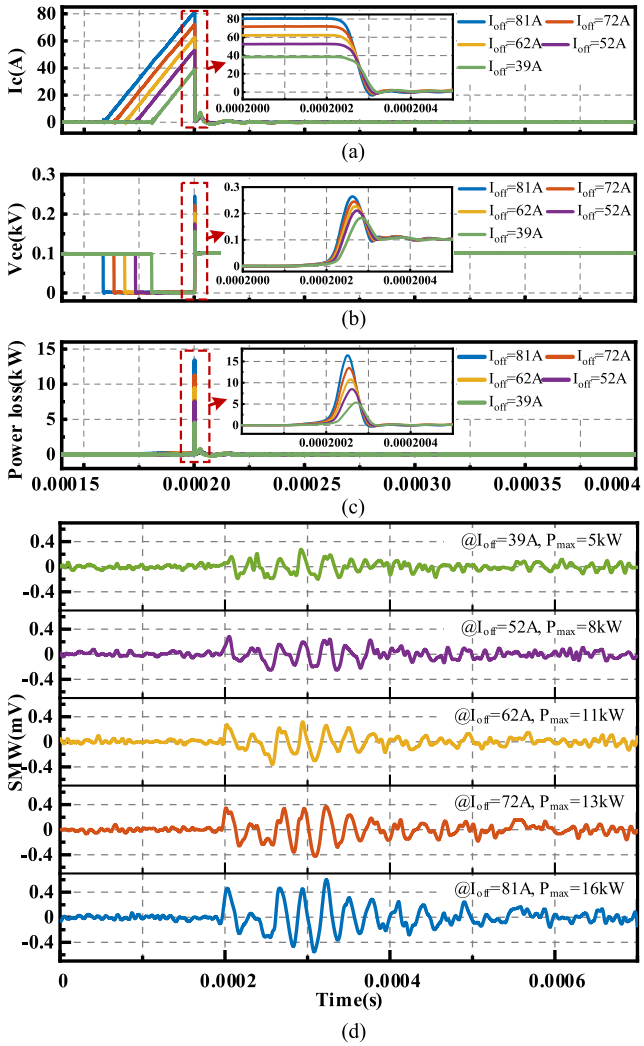

Fig. 12. SMW signals with different switching parameters. (a) Collector loading current curves. (b) Voltage between collector and emitter. (c) Power loss curves. (d) Corresponding SMW signals.

in Fig. 13. Specifically, the energy of SMW signal is defined as follows:

$$E = \int_{T_1}^{T_2} V(t)^2 dt \tag{13}$$

where $V(t)$ represents the SMW signal value, T_1 is the vibration starting moment, and T_2 is the moment when the SMW signal decays to zero. The results show that the three physical quantities, which reflect the SMW intensity including signal amplitude, peak-to-peak value, and energy present significantly positive correlation with switching-OFF moment current I_{OFF}, power pulse peak value P_{max}, and injected energy E_i, which are also consistent with the results of previously reported study [26].

D. Field Distribution Characterization

With the aid of an electronically controlled scanning platform, field reconstruction is implemented to characterize the SMW

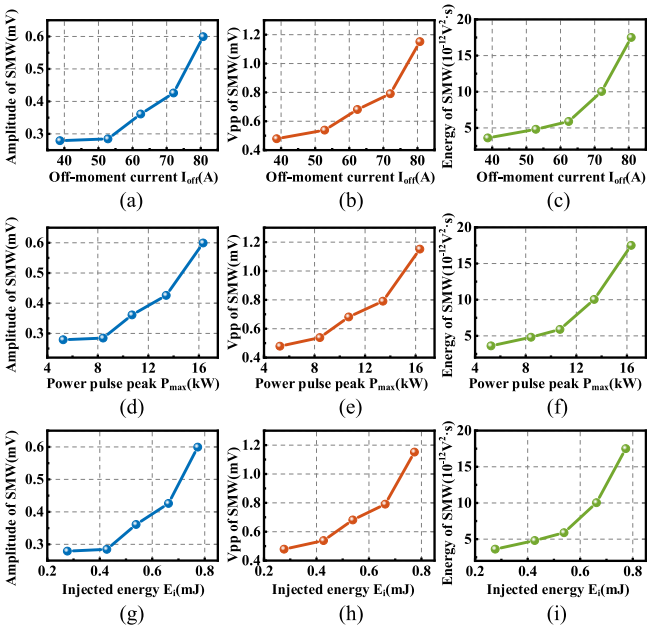

Fig. 13. Dependency of SMW intensity on switching parameters. (a) Amplitude versus I_{OFF}. (b) V_{pp} versus I_{OFF}. (c) Energy versus I_{OFF}. (d) Amplitude versus P_{max}. (e) V_{pp} versus P_{max}. (f) Energy versus P_{max}. (g) Amplitude versus E_i. (h) V_{pp} versus E_i. (i) Energy versus E_i.

field distribution on the surface of IGBT bare dies. Considering the size of the IGBT bare die used in the experiment is 9 mm×10 mm, in order to distinguish the bonding wires, the scanning points in the *X* and *Y*-directions are set to be 50 and 10, respectively. The corresponding spatial resolution along *X*-direction is 0.18 mm and 1 mm for *Y*-direction, which are enough to distinguish the bonding wires from the IGBT bare die.

The reconstruction procedure is illustrated in Fig. 14. First, the laser detection system acquires the original vibration signals of all the scanning points on entire chip surface and then uploads the data to LabVIEW interface for storage (see step 1 in Fig. 14). Then, the disordered vibration data obtained by scanning is matched to the actual spatial position of the IGBT bare die (see step 2 in Fig. 14). Afterwards, the extraction algorithm combining segmented sliding average filtering and empirical mode decomposition proposed in the previous section is adopted to remove unrelated signal components and separate out pure SMW signal (see step 3 in Fig. 14). Subsequently, the signal characteristics of SMW including amplitude, peak-to-peak value, and energy can be readily extracted (see step 4 in Fig. 14) and arranged in a storage matrix for further reconstruction (see step 5 in Fig. 14). In order to enhance the visual performance of reconstructed field maps, a piecewise cubic spline interpolation strategy is adopted. Finally, after cubic spline interpolation, the visualized field maps can be reconstructed (see step 6 in Fig. 14).

The reconstructed field distribution maps of the three physical parameters that reflect SMW intensity including amplitude, peak-to-peak value, and energy are carried out, as shown in Fig. 15. It can be seen that the middle region of the IGBT bare die suffers from relatively larger SMW compared to the edge area, which intuitively and clearly reflects the distribution characteristics of SMW on its surface. This distribution characteristic can be

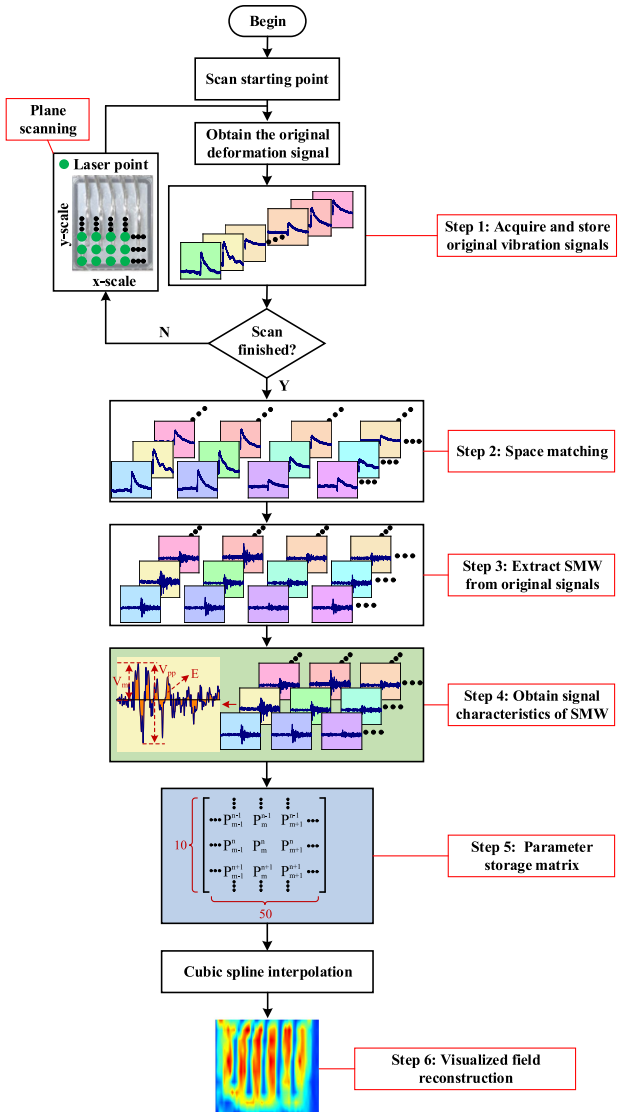

Fig. 14. Flow chart of the reconstruction process for the visualization of SMW field distribution.

explained from the perspective of wave propagation theory. To be specific, the IGBT bare die is the source of SMW in the whole packaging module, in which the vibration energy propagates in the form of wave from near to far. When propagating to the edge area of the bare die, the acoustic wave of SMW will be divided into two parts, i.e., the transmissive wave and the reflection wave. The transmissive wave penetrates through the edge area and leaks into the packaging substrate structure, while the reflection wave is reflected back into the middle region of the bare die. It can be seen that the middle region of IGBT bare die has relatively less transmissive wave energy leaking into packaging substrate structure compared with the edge area. Meanwhile, due to the concentration and superposition of the reflection waves coming back from the edge area, the vibration energy in the middle region is enhanced. Therefore, the middle region of the IGBT bare die exhibits relatively larger SMW compared to the edge area. Notably, the highest spatial resolution up to 20 μm could be readily achieved by increasing the number of scanning points, while this action will inevitably lead to a decrease in

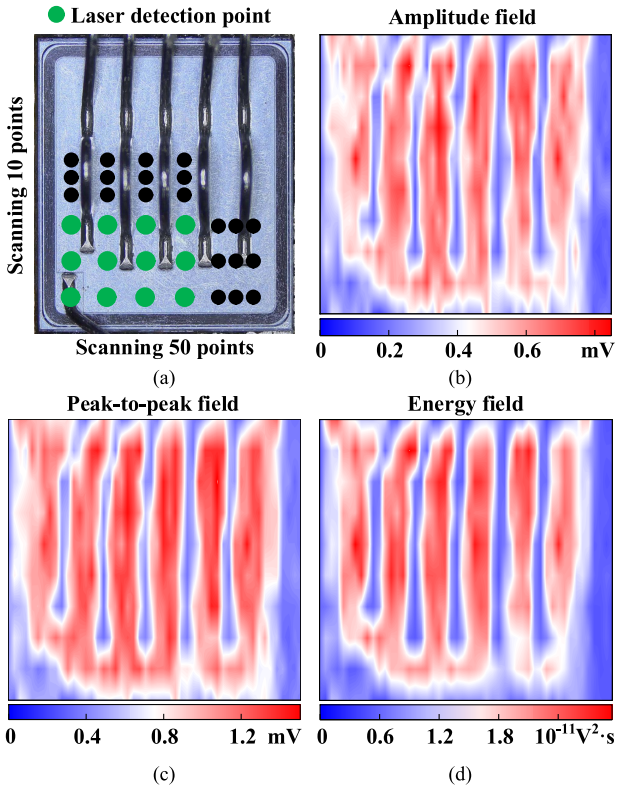

Fig. 15. Field characterization on IGBT bare die. (a) Schematic illustration of scanning setting. (b) Amplitude field distribution. (c) Peak-to-peak field distribution. (d) Signal energy field distribution.

detection efficiency. Therefore, there is a trade-off between spatial resolution and detection efficiency in the actual detection procedure. In general, above setup with 500 observation points is enough to realize field distribution characterization of SMW.

V. Limitations and Future Work

It is worth noting that the proposed method in this article has certain limitations in actual applications. Due to the detection principle of laser interference, the IGBT sample needs to be in open state without shell and silicone gel to ensure the validity of the detection. These characteristics make it difficult for the developed system to meet the detection demand of potting or molding power modules, which are well packaged. For such application scenarios, we have to admit that the proposed method can hardly deal with them. Nevertheless, it is also worth noting that the proposed method in this article has its unique application prospects. Notably, as we have stated in the introduction part of the manuscript, for the purposes of mechanism revelation, accurate physical characteristic extraction, and further exploration of SMW effect, the IGBT device used for testing does not involve potting or packaging. Therefore, for such application scenarios, the proposed method in this article has significant advantages in realizing direct capture of SMW with high spatial resolution. Besides, it is worth noting that although this work mainly focuses on SMW induced by turn-OFF energy injection to verify the effectiveness of the proposed method, the method is also equally applicable to the investigation of SMW induced by turn-ON energy injection in IGBT modules. Further investigation of the relationship between the turn-ON switching parameters and the SMW characteristics is also scheduled in our future plan to make the whole research more thorough and comprehensive.

VI. Conclusion

In this article, we developed an effective detection method based on adaptive laser interferometric vibrometer to directly capture SMW on IGBT bare dies. The proposed extraction algorithm combining segmented sliding average filtering and empirical mode decomposition achieves accurate acquisition of weak SMW signal. Based on this approach, the relationship between the SMW and electrical switching parameters of IGBT chips is carried out, suggesting that the intensity of SMW exhibits significantly positive correlation with the turn-OFF power dissipation of IGBT devices. Furthermore, field distribution characteristic of SMW is also investigated with the aid of electrical positioning and scanning platform. The results show that the middle region of the IGBT bare die suffers from relatively larger SMW compared to the edge area. This work is bound to facilitate further fundamental exploration of SMW effect in power electronic devices.

References

[1] M. Schweizer and J. W. Kolar, "Design and implementation of a highly efficient three-level T-type converter for low-voltage applications," *IEEE Trans. Power Electron.*, vol. 28, no. 2, pp. 899–907, Feb. 2013.

[2] U. M. Choi, F. Blaabjerg, and K. B. Lee, "Study and handling methods of power IGBT module failures in power electronic converter systems," *IEEE Trans. Power Electron.*, vol. 30, no. 5, pp. 2517–2533, May 2015.

[3] J. Yang, Z. He, J. Ke, and M. Xie, "A new hybrid multilevel DC-AC converter with reduced energy storage requirement and power losses for HVDC applications," *IEEE Trans. Power Electron.*, vol. 34, no. 3, pp. 2082–2096, Mar. 2019.

[4] B. Rannestad, S. Munk-Nielsen, K. Gadgaard, and C. Uhrenfeldt, "Statistical method of estimating semiconductor switching transition time enabling condition monitoring of megawatt converters," *IEEE Trans. Instrum. Meas.*, vol. 69, no. 6, pp. 3654–3665, Jun. 2020.

[5] Y. He et al., "An overview of acoustic emission inspection and monitoring technology in the key components of renewable energy systems," *Mech. Syst. Signal Proc.*, vol. 148, no. 107146, pp. 1–41, Feb. 2021.

[6] S. Levikari, T. J. Karkkainen, C. Andersson, J. Tamminen, and P. Silventoinen, "Acoustic phenomena in damaged ceramic capacitors," *IEEE Trans. Ind. Electron.*, vol. 65, no. 1, pp. 570–577, Jan. 2018.

[7] S. Zhou, L. Zhou, and P. Sun, "Monitoring potential defects in an IGBT module based on dynamic changes of the gate current," *IEEE Trans. Power Electron.*, vol. 28, no. 3, pp. 1479–1487, Mar. 2013.

[8] A. Singh, A. Anurag, and S. Anand, "Evaluation of Vce at inflection point for monitoring bond wire degradation in discrete packaged IGBTs," *IEEE Trans. Power Electron.*, vol. 32, no. 4, pp. 2481–2484, Apr. 2017.

[9] L. Dupont, Y. Avenas, and P. -O. Jeannin, "Comparison of junction temperature evaluations in a power IGBT module using an IR camera and three thermosensitive electrical parameters," *IEEE Trans. Ind. Appl.*, vol. 49, no. 4, pp. 1599–1608, Aug. 2013.

[10] Z. Xu, F. Xu, and F. Wang, "Junction temperature measurement of IGBTs using short-circuit current as a temperature-sensitive electrical parameter for converter prototype evaluation," *IEEE Trans. Ind. Electron.*, vol. 62, no. 6, pp. 3419–3429, Jun. 2015.

[11] N. M.-K. Nguyen, S. Nakajima, T. Iizuka, Y. Mita, and K. Asada, "Noninvasive localization of IGBT faults by high-sensitivity magnetic probe with RF stimulation," *IEEE Trans. Instrum. Meas.*, vol. 67, no. 4, pp. 745–753, Apr. 2018.

[12] C. Choe, C. Chen, S. Nagao, and K. Suganuma, "Real-time acoustic emission monitoring of wear-out failure in SiC power electronic devices during power cycling tests," *IEEE Trans. Power Electron.*, vol. 36, no. 4, pp. 4420–4428, Apr. 2021.

[13] S. Müller, C. Drechsler, U. Heinkel, and C. Herold, "Acoustic emission for state-of-health determination in power modules," in *Proc. 13th Int. Multi-Conf. Syst., Signals Devices*, Leipzig, Germany, Mar. 21–24, 2016, pp. 468–471.

[14] Z. Zhang et al., "Online condition monitoring of solder fatigue in a clip-bonding SiC mosfet power assembly via acoustic emission technique," *IEEE Trans. Power Electron.*, vol. 38, no. 2, pp. 1468–1478, Feb. 2023.
[15] R. M. White, "Generation of elastic waves by transient surface heating," *J. Appl. Phys.*, vol. 34, no. 12, pp. 3559–3567, Dec. 1963.
[16] L. W. Morland, "Generation of thermoelastic stress waves by impulsive electromagnetic radiation," *AIAA J.*, vol. 6, no. 6, pp. 1063–1066, Jun. 1968.
[17] H. E. Gascoigne and I. K. Mcivor, "Stress waves in layered thermoelastic media generated by impulsive energy deposition," *AIAA J.*, vol. 9, no. 5, pp. 937–943, May 1971.
[18] T. J. Karkkainen et al., "Acoustic emission in power semiconductor modules-first observations," *IEEE Trans. Power Electron.*, vol. 29, no. 11, pp. 6081–6086, Nov. 2014.
[19] T. J. Karkkainen, J. P. Talvitie, M. Kuisma, P. Silventoinen, and E. Mengotti, "Acoustic emission caused by the failure of a power transistor," in *Proc. 30th Annu. IEEE Appl. Power Electron. Conf. Expo.*, Charlotte, NC, USA, Mar. 15–19, 2015, pp. 2481–2484.
[20] P. Davari, O. Kristensen, and F. Iannuzzo, "Investigation of acoustic emission as a non-invasive method for detection of power semiconductor aging," *Microelectronics Rel.*, vol. 88–90, pp. 545–549, Sep. 2018.
[21] A. Bejger, M. Kozak, and R. Gordon, "The use of acoustic emission elastic waves as diagnosis method for insulated-gate bipolar transistor," *J. Mar. Eng. Technol.*, vol. 19, no. 4, pp. 186–196, Sep. 2020.
[22] R. Gordon and A. Bejger, "Effect of temperature change on acoustic emission signal in IGBT transistors of marine propulsion system converters," *Energies*, vol. 15, no. 12, pp. 1–14, Jun. 2022.
[23] M. Li et al., "Acoustic emission-based experimental analysis of mechanical stress wave in IGBT device," *IEEE Sens. J.*, vol. 20, no. 11, pp. 6064–6074, Jun. 2020.
[24] X. Geng et al., "Analysis of influence parameters of stress wave at the turn-off moment in IGBT device based on differential AE sensor," *IEEE Sens. J.*, vol. 22, no. 3, pp. 2259–2270, Feb. 2022.
[25] X. Geng, Y. He, G. Wang, L. Tang, Q. Li, and S. Liu, "Investigation of the influence of temperature on stress waves at the turn-off moment in IGBT," *IEEE Trans. Instrum. Meas.*, vol. 72, May 2023, Art. no. 3504509.
[26] X. Geng et al., "Theoretical study on the generation of switching stress waves in power semiconductor devices," *IEEE Trans. Power Electron.*, vol. 38, no. 3, pp. 3939–3950, Mar. 2023.
[27] M. Kozak and R. Gordon, "Experimental investigations of monolithic IGBT transistor acoustic emission phenomena," in *Proc. Conf. Comput. Appl. Elect. Eng.*, Poznan, PL, Apr. 15, 2019, Art. no. 01036.

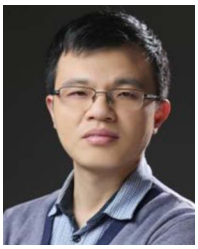

Libing Bai received the B.S. degree in automation and Ph.D. degree in testing and measuring techniques and instruments from the University of Electronic Science and Technology of China, Chengdu, China, in 2008 and 2013, respectively.

He was a Visiting Research Scholar with Newcastle University, Newcastle upon Tyne, U.K. He is currently a Professor with the School of Automation Engineering, University of Electronic Science and Technology of China. His current research interests include nondestructive testing and prognostics and health management of structure and electronic equipment.

Jiahao Wang received the B.S. degree in automation from Xinjiang University, Xinjiang, China, in 2020. He is currently working toward the Ph.D. degree in instrument science and technology with the School of Automation Engineering, University of Electronic Science and Technology of China, Chengdu, China.

His current research interests include thermal reliability analysis, mechanical reliability analysis, and diagnostics techniques for power electronic devices.

Cong Chen received the B.S. degree in electronic science and technology and Ph.D. degree in instrument science and technology from Chongqing University, Chongqing, China, in 2013 and 2018, respectively.

He is currently an Associate Research Fellow with the School of Automation Engineering, University of Electronic Science and Technology of China, Chengdu, China. His current research interests include thermal-mechanical reliability testing and evaluation of power electronics, intelligent sensing, and precise measurement.

Quan Zhou received the B.S. degree in measurement and control technology and instrument and the M.Sc. and Ph.D. degrees in measurement technology and automatic equipment from the University of Electronic and Science of China (UESTC), Chengdu, China, in 2008, 2011, and 2017, respectively.

He is currently a Senior Engineer with the School of Automation Engineering, UESTC. His current research interests include sensor testing and reliability analysis.

Jie Zhang received the B.S. degree in measurement and control technology and instrument and the M.S. and Ph.D. degrees in measurement technology and automatic equipment from the University of Electronic and Science of China (UESTC), Chengdu, China, in 2010, 2013, and 2018, respectively.

He is currently an Associate Research Fellow with the School of Automation Engineering, UESTC. His current research interests include magneto-optical sensing and its application in nondestructive testing and health management of electronics.

Lulu Tian received the B.S. degree in automation and Ph.D. degree in control science and engineering from the University of Electronic Science and Technology of China, Chengdu, China, in 2011 and 2018, respectively.

He is currently an Associate Professor with the University of Electronic Science and Technology of China. His main research interests include multisensor and multisource information fusion, machine learning, and digital signal processing.

Gen Qiu received the B.S. degree in automation and master's degree in detection technology and automation devices from the University of Electronic Science and Technology of China, Chengdu, China, in 2005 and 2009, respectively.

He is currently a Senior Engineer with the School of Automation Engineering, University of Electronic Science and Technology of China. His research interests include testing and measurement instrument design, system reliability analysis, and lifetime prediction technology.

Yuhua Cheng received the Ph.D. degree in measurement techniques and automation devices from Sichuan University, Chengdu, China, in 2007.

He is currently a Professor and the Vice Principal with the University of Electronic Science and Technology of China, Chengdu, China. His current research interests include advanced sensing and precise measurement, structural health monitoring, and complex system fault diagnosis.